Biochimica et Biophysica Acta 1864 (2016) 29–41

Contents lists available at ScienceDirect

Biochimica et Biophysica Acta

journal homepage: www.elsevier.com/locate/bbapap

Structural and biochemical characterization of two heme binding sites on α_1-microglobulin using site directed mutagenesis and molecular simulation

Sigurbjörg Rutardottir [a], Elena Karnaukhova [b], Chanin Nantasenamat [c,d], Napat Songtawee [c], Virapong Prachayasittikul [d], Mohsen Rajabi [b], Lena Wester Rosenlöf [a], Abdu I. Alayash [b], Bo Åkerström [a,*]

[a] Division of Infection Medicine, Lund University, Lund, Sweden
[b] Laboratory of Biochemistry and Vascular Biology, Division of Hematology Research and Review, Center for Biologics Evaluation and Research, Food and Drug Administration, MD, USA
[c] Center of Data Mining and Biomedical Informatics, Faculty of Medical Technology, Mahidol University, Bangkok, Thailand
[d] Department of Clinical Microbiology and Applied Technology, Faculty of Medical Technology, Mahidol University, Bangkok, Thailand

ARTICLE INFO

Article history:
Received 13 March 2015
Received in revised form 12 September 2015
Accepted 7 October 2015
Available online 21 October 2015

Keywords:
α_1-Microglobulin
Heme
Site-directed mutagenesis
Molecular simulation

ABSTRACT

Background: α_1-Microglobulin (A1M) is a reductase and radical scavenger involved in physiological protection against oxidative damage. These functions were previously shown to be dependent upon cysteinyl-, C34, and lysyl side-chains, K(92, 118,130). A1M binds heme and the crystal structure suggests that C34 and H123 participate in a heme binding site. We have investigated the involvement of these five residues in the interactions with heme.
Methods: Four A1M-variants were expressed: with cysteine to serine substitution in position 34, lysine to threonine substitutions in positions (92, 118, 130), histidine to serine substitution in position 123 and a wt without mutations. Heme binding was investigated by tryptophan fluorescence quenching, UV–Vis spectrophotometry, circular dichroism, SPR, electrophoretic migration shift, gel filtration, catalase-like activity and molecular simulation.
Results: All A1M-variants bound to heme. Mutations in C34, H123 or K(92, 118, 130) resulted in significant absorbance changes, CD spectral changes, and catalase-like activity, suggesting involvement of these side-groups in coordination of the heme-iron. Molecular simulation support a model with two heme-binding sites in A1M involving the mutated residues. Binding of the first heme induces allosteric stabilization of the structure predisposing for a better fit of the second heme.
Conclusions: The results suggest that one heme-binding site is located in the lipocalin pocket and a second binding site between loops 1 and 4. Reactions with the hemes involve the side-groups of C34, K(92, 118, 130) and H123.
General significance: The model provides a structural basis for the functional activities of A1M: heme binding activity of A1M.

1. Introduction

The Lipocalin protein family includes approximately 50 members from bacteria, plants and animals [1–3]. Although their structures are similar they have different and mostly non-related functions. A common feature is the folding of the single polypeptide into a β-barrel consisting of eight antiparallel β-strands with a closed bottom, an open end and a hydrophobic pocket which can carry small lipophilic ligands [4]. One of the members of the Lipocalin protein family, α_1-microglobulin (A1M), is a small (26 kDa), heterogeneously charged glycoprotein found in blood-plasma and interstitial fluid of all human tissues [5–7]. A1M is expressed mainly in the liver and co-synthesized with bikunin, a proteinase inhibitor and component of extracellular matrix, from the *AMBP*-gene (α_1-microglobulin-bikunin precursor protein) [8,9]. After cleavage of the precursor protein the two mature proteins are secreted separately into the blood-stream [10]. A large fraction of A1M forms complexes with other plasma proteins in blood. Approximately 50% of the protein is bound to immunoglobulin A (IgA) [11]. Less abundant complexes are formed with albumin and prothrombin [12].

The physiological function of A1M has been suggested to be protection of cells and tissues against oxidative stress induced by extracellular hemoglobin and free radicals [7]. This is supported by several recent papers, which demonstrate that A1M indeed can protect cell cultures and organ explants against oxidative damage [13–15], and therapeutic *in vivo* effects of the protein were shown in animal models of preeclampsia and hemoglobin-induced kidney damage [16,17]. Mechanistically, the antioxidative protection is achieved by reductase and radical-

Abbreviations: A1M, α_1-microglobulin; AMBP, A1M-bikunin precursor protein; IgA, immunoglobulin A; ROS, reactive oxygen species; FPLC, fast protein liquid chromatography; SPR, surface plasmon resonance; MD, molecular dynamics; CD, circular dichroism; RMSD, root mean square deviation; RMSF, root mean square fluctuation.

* Corresponding author at: Division of Infection Medicine, Lund University, Sölvegatan 19, 22184 Lund, Sweden.
E-mail address: sigurbjorg.rutardottir@med.lu.se (B. Åkerström).

http://dx.doi.org/10.1016/j.bbapap.2015.10.002
1570-9639/

binding activities of A1M, and it was shown that the C34 unpaired thiol group and the side-chains of K92, 118 and 130 of A1M are involved in the reductase and radical-binding activities [18–20]. A1M has also been shown to bind heme[1] *in vitro* and *in vivo* [21–23] and was suggested to contribute to heme degradation by a mechanism still unknown, but which involves proteolytic activation of A1M [21]. The heme binding of A1M was recently demonstrated to result in a trimeric complex with heme in a 1:2 stoichiometry [24]. Furthermore, a heme binding site, which involves the C34 thiol group and H123 imidazole ring, has been proposed based on the crystal structure of A1M [25].

Free heme in plasma and extracellular fluid is the result of degradation of hemoglobin and other proteins carrying a heme prosthetic group. The heme-group presents a potential chemical threat to the organism by generation of reactive oxygen species (ROS), which are toxic and can cause severe damage to cells and tissues [26]. We hypothesized that the above-mentioned side-chains of A1M are involved in the heme binding. To test this, we investigated wild type (Wt)-A1M and the previously constructed mutated forms of A1M: C34S- and K [3]T-A1M [27], the latter carrying Lys → Thr substitutions in positions 92, 118 and 130. We also constructed, prepared and investigated a new mutated form, H123S-A1M (Fig. 1A). The results suggest a two binding site-model where the three lysine side-chains participate in coordination of the first heme-group and the C34 and H123 side-chains coordinate the second heme-group.

2. Materials and methods

2.1. Reagents and proteins

Heme (hemin; ferriprotoporphyrin IX chloride) was purchased from Porphyrin Products, Inc. (Logan, UT, U.S.A.). Stock solutions of heme were prepared by dissolving heme in DMSO to 10 mM and used within 10 h. Clarity Western ECL Substrate was from Bio-Rad Bio-Rad Laboratories (Hercules, CA, USA). Heme-agarose was from Sigma-Aldrich, Sweden. Sepharose CL-4B was from GE Healthcare, Sweden. Pierce BCA Protein Assay kit from Thermo Scientific, Sweden. AcroPrep Advance 96 Filter Plate 1.2 μM supor® was from PALL Corporation (Port Washington, NY, USA), and Nunc TM 96-Well Microplates were purchased from Thermo Scientific.

2.2. Recombinant A1M

Wild-type (Wt) and mutated variants of A1M were expressed in *Escherichia coli* (*E. coli*) as described [27]. Using site-directed mutagenesis a Cys → Ser substitution was introduced at amino acid position 34 in the C34S-A1M mutant, Lys → Thr substitutions at positions 92, 118, and 130 in the K [3]T-A1M mutant, and a His → Ser substitution at position 123 in the H123S-A1M mutant. The four forms of recombinant A1M, Wt-A1M, C34S-A1M, K [3]T-A1M and H123S-A1M, were purified and refolded as described [27] with the addition of ion-exchange chromatography and size exclusion purification steps as follows. The protein solution was applied to a column of DEAE-Sephadex A-50 (GE Healthcare, Uppsala, Sweden) equilibrated with the starting buffer (20 mM Tris–HCl, pH 8.0). A1M was eluted at a flow rate of 1 ml/min using a linear pH gradient consisting of 250 ml starting buffer and 250 ml elution buffer (20 mM Tris–HCl, 0.5 M NaCl, pH 8.0). Size-exclusion chromatography was run on a Superose 12 column obtained from GE Healthcare using Äkta purifier 10 system (GE Healthcare) run at a flow-rate of 1 ml/min. Wt-A1M without the N-terminal His_8-tag was a generous gift from A1M-Pharma AB.

[1] The term "heme" is used in this article to denote both the ferrous and ferric forms.

2.3. Secondary structure estimation by far-UV circular dichroism

The secondary structure of A1M variants was determined with a Jasco-J810 spectropolarimeter instrument using a 2 mm quartz cuvette at continuous mode at speed 20 nm/min, band width of 1 nm and a 1 nm resolution. Temperature was held at 22 °C by a Peltier thermostat. The concentration of protein was 10 μM in 20 mM Tris–HCl pH 8.0 + 0.15 M NaCl. Each spectrum is a mean of five replicates. After subtraction of the buffer spectrum and recalculation into mean residue molar elipticity units, the CD spectra were analyzed using the CDPro package to determine different secondary structure content [28].

2.4. Spectrophotometric analysis of heme binding

Absorbance spectra were measured on a Beckman (Beckman Instruments, Fullerton, CA) DU 800 spectrophotometer using a scan rate of 1200 nm/min in the UV–VIS region between 250 and 700 nm at 22 °C. The protein concentration was 10 μM in 20 mM Tris–HCl, pH 8.0, 0.15 M NaCl, which was also used as blank. Heme was dissolved in DMSO to 10 mM and diluted in 20 mM Tris–HCl, pH 8.0, 0.15 M NaCl to 3 mM. Volumes of this stock solution were then added to each protein solution, to a final concentration 20 μM. Blanks with equivalent concentration of DMSO were used for samples with heme. Protein solutions were scanned immediately after mixing with heme and after 1 h or 24 h.

2.5. Fluorescence spectroscopy

Fluorescence measurements were performed using a Jasco J-810 spectropolarimeter (equipped with a FMO-427 monochromator) with a 100 μl quartz cuvette (Hellma Precision Cell, Type no. 105.251-QS, light-path length 3 mm in both excitation and emission modes) under nitrogen flow. Temperature was held at 22 °C by a Peltier thermostat. Tryptophan fluorescence was measured by exciting at wavelength 295 nm. Fluorescence emission was detected from 310 to 400 nm with slits set at 5 nm bandpass. Emission spectra were recorded three times, averaged, and the peak at 346 nm was measured. A1M protein concentration was 1 μM in 20 mM Tris–HCl, pH 8.0, 0.15 M NaCl. At this concentration, the fluorescence signal of the protein was well resolved within the detector sensitivity (set at 900 V). The emission spectra of the protein solution (100 μl) without heme were recorded first and subsequently heme from a stock-solution was added (1 μl at a time, up to 4 μl). Blank subtractions were made for Tris–HCl, pH 8.0, 0.15 M NaCl since the concentration of DMSO did not affect the emission spectra.

2.6. Induced circular dichroism

All samples containing heme were evaluated for the protein-induced chirality in the near-UV to visible CD range of 300–700 nm (referred to as visible CD). The visible CD measurements were performed on a Jasco J-815 Spectropolarimeter (JASCO Co., Japan) with the temperature maintained at 25 ± 0.5 °C. The spectra were recorded using a scan speed of 100 nm/min, bandwidth of 1.0 nm, and resolution of 0.2 nm, and accumulated in triplicate. A protein alone (Wt-A1M or mutant, respectively) was used as a blank. To accumulate the induced CD, A1M was used at an initial protein concentration of ~45 μM, and the measurements were performed in a quartz cuvette with 1 cm pathlength. Heme content in the samples varied from ~4.5 μM to ~50 μM by using calculated amounts of the heme 2 mM stock solution in DMSO. The content of DMSO in the mixed samples did not exceed 4%. An ellipticity of induced CD spectra was expressed in millidegrees (mdeg).

2.7. Analytical size exclusion chromatography

Samples were size-fractionated on a Superose 12 10/300 fast protein liquid chromatography (FPLC) column (GE Healthcare, Uppsala,

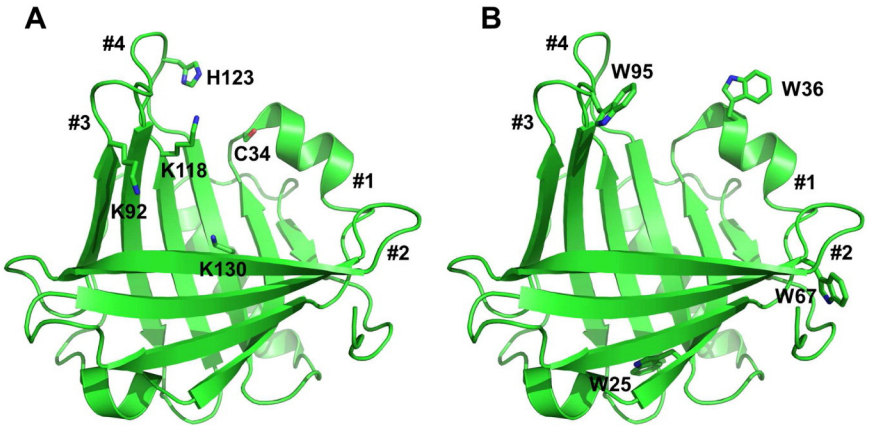

Fig. 1. Three-dimensional structure of A1M. The illustration was generated using PyMOL [32] and coordinates from the crystal structure of human A1M [25]. β-strands and α-helices are shown as green ribbons. The four loops at the open end of the lipocalin pocket are labeled #1–#4. (A) Side-chains of C34, K92, K118, K130 and H123 are shown in green sticks. (B) Side-chains of W25, W34, W67 and W95 are shown in green sticks.

Sweden). A1M/heme molar ratio was 1:2. Heme was dissolved in DMSO to 10 mM and added from a 3 mM stock solution prepared as described above. 500 μl of sample was applied to the column after 1 h of incubation with heme. The proteins were eluted with 20 mM Tris–HCl, pH 8.0, 0.15 M NaCl and run at 0.5 ml/min. Fractions of 0.5 ml were collected.

2.8. Native PAGE and Western blot of A1M incubated with heme

A1M (5 μM) in 20 mM Tris–HCl, pH 8.0 + 0.15 M NaCl was incubated for 30 min or 24 h with 50, 10 and 0.1 μM heme. Samples were mixed with equal amounts of sample buffer for native PAGE, pH 6.8, and subjected to 12% Criterion™ TGX™ Precast Gels (Bio-Rad). The gels were either stained with Coomassie Brilliant Blue R-250 (BDH Chemicals, Ltd. Poole, UK) or transferred to polyvinylidene difluoride (PVDF) membranes using Trans-Blot Turbo system from Bio-Rad. The membranes were incubated in Clarity Western ECL Substrate and imaged with a digital imager (BioRad).

2.9. Binding of A1M to heme-agarose

Beads of heme-agarose and Sepharose were washed three times with an excess of 10 mM Tris–HCl pH 8.0 + 0.125 M NaCl, yielding a final 1:1 suspension in this buffer. The proteins were diluted in 10 mM Tris–HCl pH 8.0 + 0.125 M. Dilution series of all proteins were made to final concentrations of 10, 7.5, 5, 2.5, 1.25, and 0.625 μM. Seventy-five μl were then transferred to Nunc TM 96-Well Microplates in duplicates (one set for incubation with heme agarose and control Sepharose and one without beads). Twenty μl 50% heme-agarose or Sepharose were pipetted into the wells, using large-opening pipette-tips, and the plates were incubated in RT on a shaker for 30 min. The protein/beads mixtures were then transferred to AcroPrep Advance 96 Filter Plate and spun at 2000 g for 2 min. Twenty-five μl of non-incubated samples and 25 μl of each flow-through were transferred to a new Nunc TM 96-Well Microplate, 200 μl of BCA reagent was added and the plates incubated at 37 °C for 30 min. The absorbance was measured at wavelength 550 nm, using a Multilabel Counter (Victor™ 1420 Perkin Elmer Life and

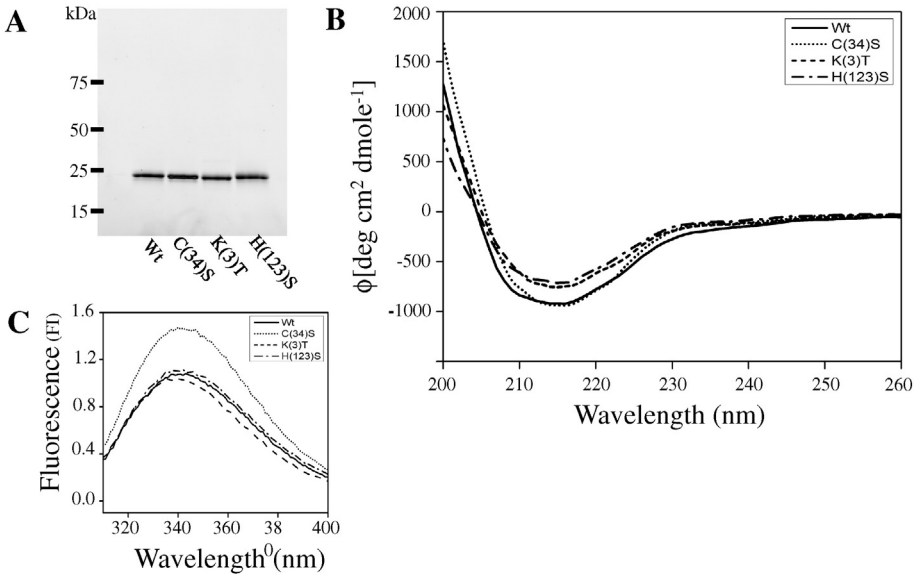

Fig. 2. Size, purity and spectroscopic properties of the four variants of recombinant A1M. (A) SDS-PAGE was performed in the presence of mercaptoethanol (T = 12%). Approximately 2 μg of Wt-A1M, C [34]S-A1M, K [3]T-A1M, and H(123)S-A1M were applied to the gel and stained with Coommassie. (B) Far-UV CD spectra of A1M variants (10 μM in 20 mM Tris–HCl, pH 8.0, 0.15 M NaCl). Similar spectra of Wt-A1M, C [24]S and K [3]-T-A1M were published in Kwasek et al. [27] and are included here for comparison of H(123)S-A1M. (C) Fluorescence spectra of A1M variants (1 μM) in 20 mM Tris–HCl, pH 8.0, 0.15 M NaCl).

Table 1
Secondary structure prediction of recombinant A1M-variants.

	α-Helix (%)	β-Sheet (%)	Turns (%)	Unordered (%)
Wt	4.3	43.3	22.2	30.0
C [34]S	2.0	48.6	18.6	29.6
K [3]T	1.2	44.9	20.9	32.3
H(123)S	4.2	47.2	19.5	28.9

Analytical Sciences, Turku, Finland). Statistical analysis was performed using OriginPro 9.0 software (Microcal, Northampton, MA, USA).

2.10. Catalase-like activity assay

Monitoring of the Soret band intensity of heme equimolar samples with A1M mutants (C34S, K(3)T, H123S) after adding hydrogen peroxide was performed in comparison with Wt-A1M and free heme in Tris buffer according to the procedure described earlier [29] with minor modifications. Equimolar (L/P 1.0) heme/A1M samples were prepared by adding 20 μl of heme stock solution in DMSO (2.2 mM) to 1 ml of 45 μM solutions of A1M or each of the A1M mutants. After overnight (~20 h) incubation at room temperature in dark, the samples were evaluated by UV/Vis measurements and diluted by buffer to adjust the Soret band intensity to ~0.6 AU. Heme sample in Tris buffer (with approximately the same absorbance intensity) was freshly prepared and used immediately. These UV/Vis spectra served as initial (zero time) baseline. After a 7 μl aliquot of 50 mM hydrogen peroxide was added to each sample, the time course of spectral changes were measured at 30 s, 1 min, 2 min, 4 min, 6 min, 8 min and 10 min.

2.11. Surface plasmon resonance (SPR)

SPR experiments were conducted on Biacore T200 (GE Healthcare, Piscataway, NJ). Anti-His mouse IgG1 monoclonal antibodies (R&D Systems, Minneapolis, MN) were immobilized on CM5 sensors by amine coupling, ~18,000 response units (RU). The tagged proteins were injected at a flow of 10 μl/min for 360 s. Prior to injection, a freshly prepared heme solution in DMSO was subjected to serial double dilutions using PBS buffer to create a range of eight heme concentrations, from 100 μM down to 0.625 μM. Heme preparations were injected over captured A1M variants for 2 min with a flow 30 μl/min at 25 °C, and the association was recorded, followed by the dissociation monitored during 10 min. Data were analyzed using the Biacore T200 evaluation software (GE Healthcare), subtracting the reference surface and buffer control signals from each curve. Data were globally fitted by simultaneous numerical integration to the association and dissociation parts of the interaction, using the heterogeneous ligand kinetic analysis models (T200 BIAevaluation software, version 1.0; Biacore AB, Uppsala, Sweden).

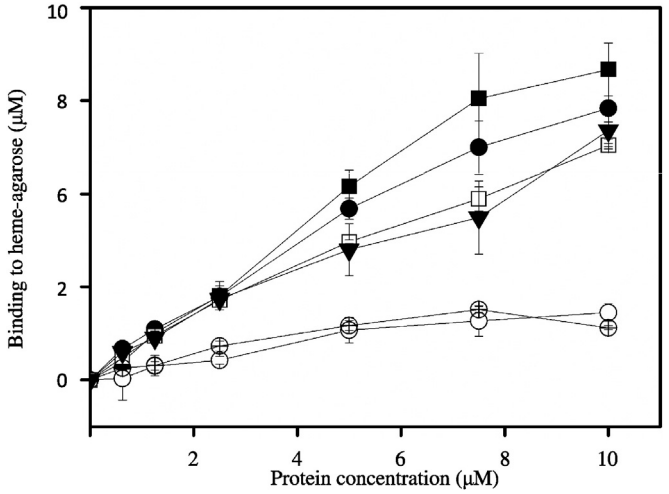

Fig. 4. Binding of A1M-variants to heme-agarose. The proteins were diluted in 10 mM Tris–HCl pH 8.0, 0.125 M NaCl. Dilution series of all proteins (concentrations of 10, 7.5, 5, 2.5, 1.25, 0.625 μM) were incubated with heme agarose and unconjugated Sepharose for 30 min. Beads and unbound protein were separated by centrifugation through a filter plate. Non-incubated samples and each flow through, containing unbound protein, were analyzed with BCA Protein Assay Kit. Binding to unconjugated Sepharose was used as control. Binding to heme-agarose is shown as follows: ■: Wt, ●: C [34]S, □: K [3]T,▼: H(123)S, ⊗: Ovalbumin. ○:Wt-A1M to un-conjugated Sepharose. The mean of two replicates +/− SEM are shown.

2.12. Molecular simulation of A1M-heme binding

A representative molecular structure of heme (accession number HEB) was obtained from PDBeChem [30] as a MOL file. Molecular volume was subsequently computed from the MOL file of heme b *via* the online tool from Molinspiration [31]. Briefly, the method for computing

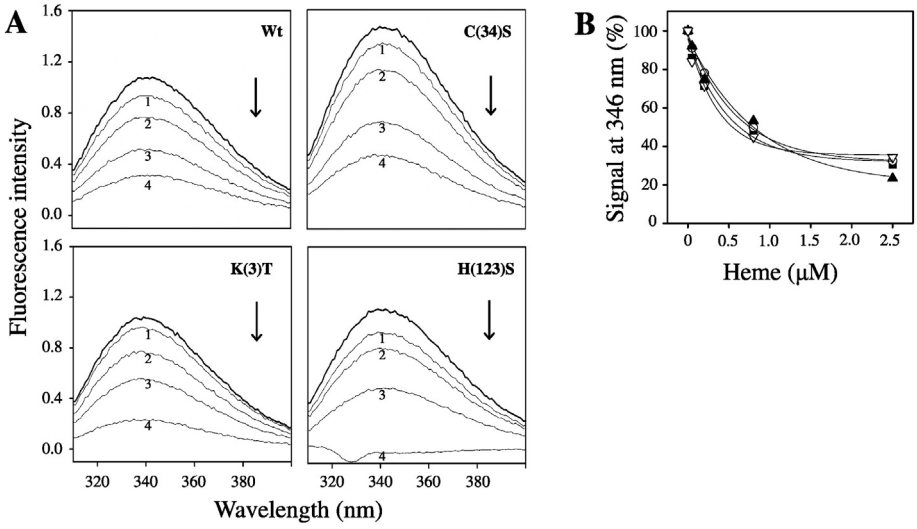

Fig. 3. Heme-induced tryptophan fluorescence quenching in the four A1M-variants. (A) Fluorescence spectra of A1M-variants (1 μM) incubated with heme to a final concentration of; 1 = 0.05, 2 = 0.2, 3 = 0.8, 4 = 2.5 μM. (B) Normalized titration curve of A1M-variants with heme. The fluorescence intensity of each A1M-variant without heme-addition was set to 100%. The data were fitted to lines with the equations $y = 31.9 + 64^{*}e^{-0.0020^{*}x}$ (wt), $y = 31.9 + 66^{*}e^{-0.0017^{*}x}$ (C34S), $y = 20.2 + 76^{*}e^{-0.0012^{*}x}$ (K3T), and $y = 35.5 + 61^{*}e^{-0.0026^{*}x}$ (H123S). n:Wt, ¡: C(34)S,s: K(3)T,▲: H(123)S.

Table 2
Kinetic rate constant and dissociation constants determined by SPR for the heme interactions with A1M variants.

A1M	k_a (M^{-1} s^{-1})	k_d (s^{-1})	K_D (M)[a]
Wt[b]	568.25	7.69×10^{-3}	$13.55 \times 10^{-6} \pm 0.4$
C34S	557.40	6.21×10^{-3}	$11.17 \times 10^{-6} \pm 0.9$
K [3]T	655.55	5.89×10^{-3}	$9.03 \times 10^{-6} \pm 0.9$
H123S	608.15	6.79×10^{-3}	$11.20 \times 10^{-6} \pm 0.8$

[a] All the kinetics parameter were analyzed using the Biaevaluation software, version 4.1.1. The data were fitted using 1:1 L binding model represented by equation (A + B AB).
[b] Previously published in Karnaukhova et al. ref. 43.

the molecular volume is based on group contributions in which the sum of fragment contributions were fitted to actual three-dimensional molecular volume of a training set comprising twelve thousand molecules [32]. The three-dimensional molecular structures of the training set were geometrically optimized using the semi-empirical Austin Model 1 (AM1) method.

In reconstructing the wild-type structure of A1M, residue 34 of the crystal structure (PDB ID: 3QKG) was mutated from serine to cysteine using PyMOL [33]. This was performed whereby the rotamer was independent of the backbone such that the sulfhydryl moiety is pointed towards the imidazole moiety of H123. Molecular volume of the lipocalin pocket in the crystal structure of A1M was computed using CASTp [34].

A query on Protein Data Bank for structures having the lipocalin SCOP fold yielded 280 hits, of which 46 contained a bound heme. From this, 45 are either nitrophorin 1, 2 or 4 from *Rhodnius prolixus* (PDB ID: 1D2U, 1D3S, 1EUO, 1IKE, 1IKJ, 1KOI, 1NP1, 1NP4, 1PEE, 1PM1, 1SXU, 1SXW, 1SXX, 1SXY, 1SY0, 1SY1, 1SY2, 1SY3, 1T68, 1U0X, 1U17, 1U18, 1X8N, 1X8O, 1X8P, 1X8Q, 1YWA, 1YWB, 1YWC, 1YWD, 2A3F, 2ACP, 2AH7, 2AL0, 2ALL, 2AMM, 2ASN, 2AT0, 2EU7, 2GTF, 2HYS, 2NP1, 3C76, 3NP1, 4NP1) while the other was a nitrophorin-like protein from *Arabidopsis thaliana* (PDB ID: 3EMM). The former set constitutes amino acid length of 179–184 while the latter structure had 153 residues. Furthermore, owing to the fact that the former set of 45 structures spanned similar length, it was selected for further analysis. Structural alignment was performed using MultiProt [35].

The structure of wild-type A1M was docked to heme using HADDOCK [36]. A second heme was subsequently docked to a putative heme binding site, which is formed by axial ligands comprising of C34 and H123 as proposed by Meining and Skerra [25] of the top-scoring model using PyMOL. The structure of A1M-heme complex was then refined using the energy-minimization in gas phase followed by molecular dynamics (MD) simulation on GROMACS, version 4.0 [37]. During the refinement, the distance restraints of the side chain of C34 and H123 with the second heme were applied, and inappropriate bond lengths of any atom were fixed. The simulation was performed on the explicit-solvent periodic boundary conditions under the NPT condition at 300 K of temperature using the modified Berendsen thermostat [38] and 1 bar of pressure using Parrinello-Rahman barostat [39]. GROMOS96-53A6 force field was applied for both protein and heme structures and the ionization states of amino acid residues were set according to the standard protocol [40]. The SPC water was used as a solvent model. Bond lengths were constrained using LINCS algorithm that allows for a 2.0 fs-time step [41]. A cut-off distance for the short-range neighbor list was set to 0.9 and 1.4 nm for the electrostatic and van der Waals interactions, respectively. Long-range electrostatic interactions are approximated using PME method [42].

The same MD protocol was also applied for further analyzing dynamic properties of A1M-heme complex. For the data collection, atomic coordinates were recorded every 10 ps.

3. Results

3.1. Expression and characterization of A1M-mutants

The mutated side-group residues are high-lighted in Fig. 1A. Before measuring the heme binding of the mutated A1M-variants, purity and

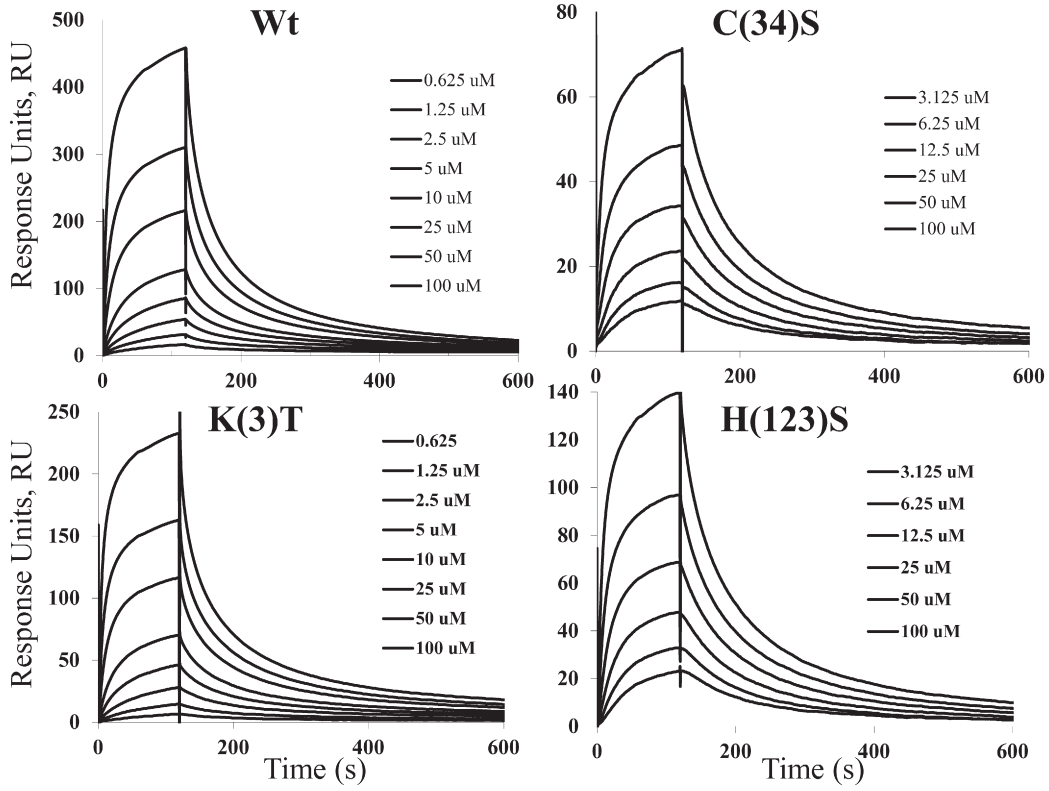

Fig. 5. Binding of heme to A1M analyzed by surface plasmon resonance. Sensorgrams of the heme binding to wt-, C [34]S-, K [3]T- and H(123)S-A1M captured by the anti-His mouse IgG1 monoclonal antibody immobilized on CM5 sensor chip. Increasing signals were obtained using 0.625–100 μM heme.

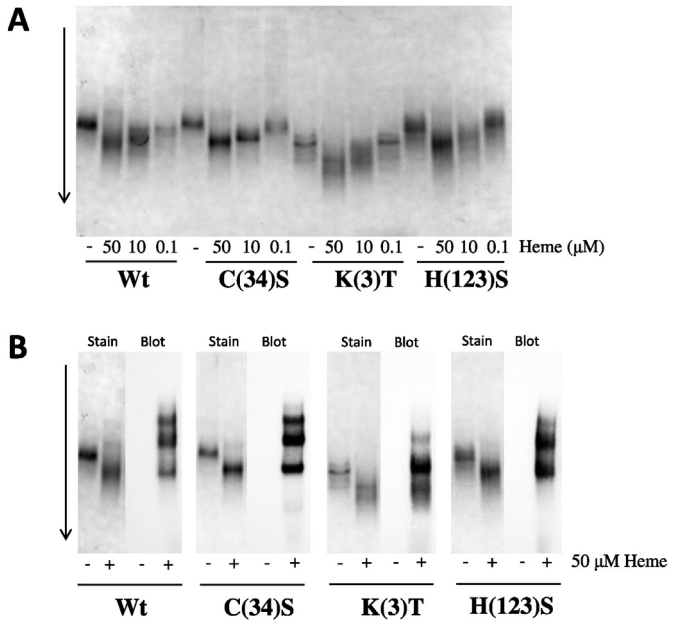

Fig. 6. Heme-induced migration shift of A1M-variants. (A) Native PAGE of A1M (5 μM) in 20 mM Tris–HCl, pH 8.0, + 0.15 M NaCl incubated for 1 h with 50, 10 or 0.1 μM heme. Samples were mixed with equal amounts of sample buffer for native PAGE, pH 6.8, and subjected to a 12% Criterion™ TGX™ Precast Gel and stained with Coommassie. (B) Peroxidase blotting of A1M-variants incubated for 4 h without or with heme (50 μM), subjected to native PAGE in a 12% Criterion™ TGX™ Precast Gel and thereafter either stained with Coomassie (5 μg A1M), or transferred to polyvinylidene difluoride (PVDF) membranes (2 μg A1M). The membrane was incubated in Clarity Western ECL Substrate and imaged with a digital imager (BioRad).

basic structural properties were analyzed by SDS-PAGE, far-UV CD spectroscopy and optical fluorescence (Fig. 2). As shown in Fig. 2A, no visible impurities could be detected. Similar apparent sizes were seen, as expected from the theoretical masses of the four variants (Wt-A1M: 22.64 kDa, C(34)S: 22.66, K [3]T: 22.56 and H(123)S: 22.59). Far-UV CD spectra of Wt-A1M and the mutated A1M-forms suggest a similar composition of secondary structure, *i.e.* mostly β-structure (Fig. 2B; Table 1). The CD spectra of the four A1M-variants were also consistent with the X-ray crystallography-derived three-dimensional structure of Wt-A1M [25]. Four tryptophan residues are found in A1M located at various positions (Fig. 1B) and tryptophan fluorescence spectra were recorded as an estimate of the overall conformation of the mutants (Fig. 2C). A higher intensity was obtained from the C [34]S-mutant, possibly as a result of an interaction between the closely located C34- and W36-residues, reducing the intensity of the fluorescence of W36 in Wt-A1M and the other mutants (Fig. 1B). Apart from this, similar spectra were obtained, suggesting no major differences in the overall conformation of the four variants.

3.2. All A1M-variants bind heme

The binding of the heme-group to the A1M-variants was first investigated by quenching of the tryptophan fluorescence during heme-titration, using a protein:heme ratio of 0.4–20 (Fig. 3A,B). The results of this experiment show that heme was bound to all variants with a similar binding strength. Quenching of 50% of the tryptophan fluorescence of 1 μM A1M was achieved in the 0.8 μM range in all cases and approximately 70% of the tryptophan fluorescence was quenched by 2.5 μM heme. Furthermore, the binding of heme to the A1M variants was analyzed using heme-agarose titration (Fig. 4) and surface plasmon resonance (SPR) (Table 2). Both techniques confirm the binding of heme by all four A1M-variants, and indicate a slightly higher binding by Wt-A1M compared to the mutated variants. Heme-agarose titration with increasing amounts of the A1M variants (Fig. 4) yielded binding responses in the order Wt-A1M > C [34]S-A1M > H(123)S-A1M and K [3]T-A1M. Ovalbumin, a negative control protein, did not bind at all to heme-agarose and Wt-A1M did not bind to un-conjugated Sepharose.

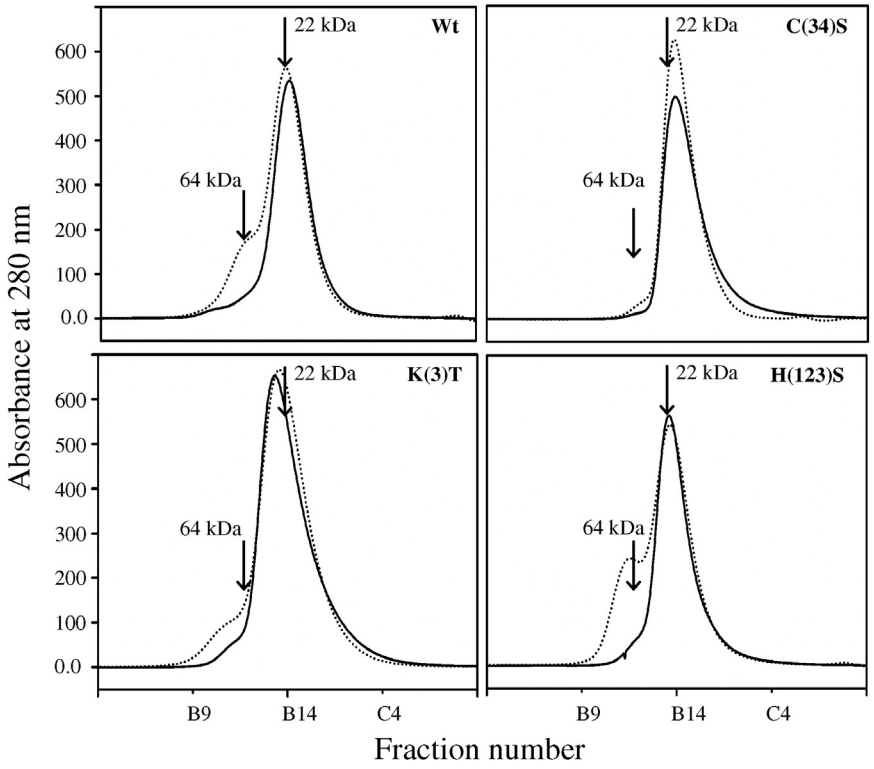

Fig. 7. Size exclusion chromatography of A1M variants incubated with heme. A1M (0.5 ml of a 44 μM-solution) was applied on a Superose 12 FPLC column and eluted with 20 mM Tris–HCl, pH 8.0, 0.15 M NaCl at 0.5 ml/min (unbroken line). A1M and heme in molar ratio of 1:2 were incubated for 1 h and run on Superose 12 FPLC column as above (dotted line). The size calibration on the column was performed with Wt-A1M (22 kDa) and with human hemoglobin (64 kDa).

The SPR data analysis, within heme concentrations 0.625–100 μM (Fig. 5), resulted in dissociation constant (K_D) values of 13.82×10^{-6} (Wt-A1M), 11.81×10^{-6} (C34S), 9.65×10^{-6} [K [3]T] and 11.74×10^{-6} (H123S) (Table 2), confirming the results of heme-agarose titration. Although these kinetic data fitted to a 1:1-binding model, SPR data obtained for an extended range of heme concentration (0.625–500 μM) fitted better to a 1:2 binding model, supporting the earlier proposed two binding site model [24]. The latter should be interpreted with care, however, since low heme solubility and its increased aggregation at high concentrations greatly limit the reliability of precise determination of kinetic constants for the low affinity binding sites [43].

3.3. Oligomerization of A1M-heme complexes

The binding of heme was studied by gel-shift assay, using native PAGE, to analyze the electrophoretic mobility of the A1M-variants alone or in the presence of 0.1, 10 or 50 μM heme (Fig. 6A). A clear migration shift was seen of all four variants and the dose-dependence was similar. These results support the findings described above, *i.e.* binding of heme with similar strength by all A1M-variants. A similar migration shift was seen with Wt-A1M without the N-terminal His-tag, and no migration shift of the control proteins α_1-acid glycoprotein and ovalbumin after heme-incubation, or of Wt-A1M in the presence of the carrier DMSO, could be seen (data not shown). To visualize the heme-group in the A1M-bands, the gels were analyzed by peroxidase-activity (ECL)-blotting (Fig. 6B). All A1M-variants displayed heme-induced peroxidase-activity after incubation with heme. Three bands were seen with all variants, probably corresponding to the monomeric, dimeric and trimeric A1M-heme complexes previously reported [24]. Interestingly, the peroxidase activity was much stronger in the dimeric and trimeric bands, when relating to the protein staining activity (Fig. 6A *vs* B).

The sizes of the A1M-heme complexes were also investigated by Superose 12 gel-filtration (Fig. 7A). Incubation for 1 h with heme (A1M:heme = 1:2) resulted in the appearance of larger forms besides the monomeric peak, suggesting an increased oligomerization of A1M in the presence of heme. This supports the results of the PAGE shown in Fig. 6. The high molecular weight-forms were most pronounced in Wt-A1M and H(123)S-A1M, and less so in K [3]T- and C [34]S-A1M. Furthermore, a slight heme-induced shift of the monomeric peak towards higher molecular mass was seen in Wt-A1M.

3.4. UV–Vis absorbance of A1M-heme is dependent on C34, K92, 118, 1(32) and H132-residues

The heme binding was followed by UV–Vis absorbance spectrophotometry (Fig. 8). The heme binding could be confirmed, but the time-dependence of the binding was different for the various A1M-forms. A broad peak with a maximum (λ_{max}) around 400 nm was seen immediately after mixing of 10 μM A1M + 20 μM heme for all variants (not shown). After 24 h, however, a red-shift of λ_{max} towards a higher wavelength was seen for Wt-A1M, but not for any of the mutants (Fig. 8A; peak values of Soret-band shown in Table 3). This red-shift was beginning after a few minutes and could be recorded at 30 min and onwards (not shown). Furthermore, zooming in on 500–700 nm wavelengths (Fig. 8B), the Wt-A1M-heme complex displayed a maximum at 540 nm, which was less pronounced in the mutants. The mutants also displayed an absorbance shoulder at 610 nm, this was most pronounced in the K [3]T-A1M-heme and H(123)S-heme complexes. The spectral differences could also be seen as a striking difference in color of the heme-complexed A1M-variants (Fig. 8C). At these concentrations (10 μM of both protein and heme), the Wt-A1M heme solution was red whereas the C [34]S-A1M heme complex was yellow and the K [3]T-A1M and H(123)S-A1M showed a similar yellow-brown color as free heme. The red-shifted Soret-band and the 540 nm-maximum are seen in ferrous (FeII) heme binding proteins [44]. These results

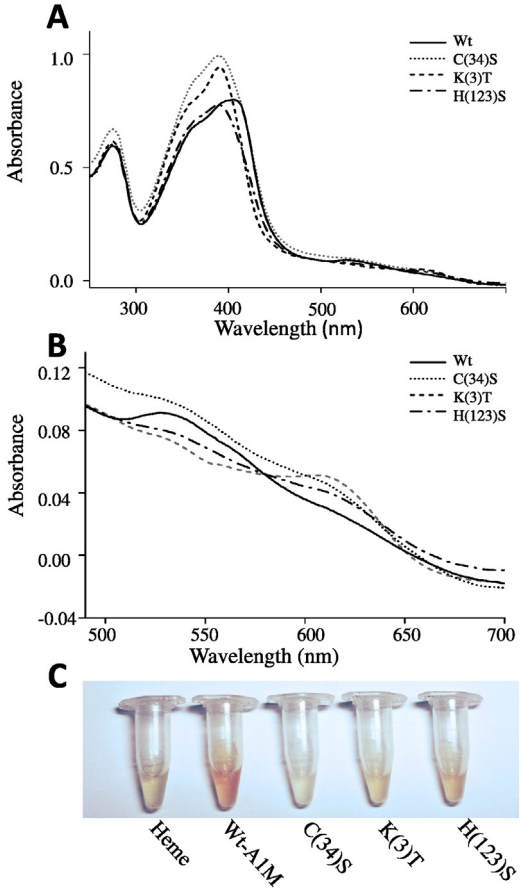

Fig. 8. Absorbance spectrophotometry of A1M variants incubated with heme. (A) Absorbance spectrum of A1M variants (10 μM) in the presence of 20 μM heme in 20 mM Tris–HCl, pH 8.0, 0.15 M NaCl after 24 h of incubation. A similar absorbance spectrum of Wt-A1M was previously published in Karnaukhova et al. [43]. (B). Close-up of the absorbance spectrum between 500 and 700 nm of A1M variants (10 μM) in the presence of 20 μM heme in 20 mM Tris–HCl, pH 8.0, 0.15 M NaCl after 24 h of incubation. (C) The A1M variants incubated with heme and heme only were also analyzed visually. Protein:heme ratio was 1:2 and the heme concentration 20 μM.

therefore suggest that A1M undergoes reducing reactions with the heme-group, involving the C34-residue and regulated by H123 and K92, 118 and 130.

To minimize the contribution of unbound heme-groups to the spectra, the monomer peak fractions of the gel filtrated A1M-heme complexes were also analyzed by UV–Vis absorbance spectrometry. The peak wavelengths of the Soret-band (λ_{max}) before and after gel filtration are shown in Table 3. The red-shift of the Wt-A1M heme

Table 3
Summary of the UV/Vis absorbance spectra and induced CD for heme complexes with A1M variants at low (heme:A1M ratio 0.1) and high (heme:A1M ratio 1.0) relative heme content.

	Heme, μM	Heme:A1M ratio	Absorbance Soret λmax, nm		Induced CD, nm
				Monomer[a] gelfiltration	
Wt	4.5	0.1	422		421
	45	1.0	414	414	403
C (3)S	4.5	0.1	397		397
	45	1.0	394	392	400, 408
K (3)T	4.5	0.1	421		417
	45	1.0	399	399	414
H(123)S	4.5	0.1	421		416
	45	1.0	390	391	393, 405

[a] The heme:A1M ratio was 2.0 before application to gel filtration column.

complex was also apparent after gel filtration, whereas the monomer fractions of three mutants showed a λ_{max} below 400 nm. This suggests that the bound heme group is reduced by Wt-A1M but not the mutated forms.

3.5. Catalase-like activity

The catalase-like activity of A1M-heme complexes was measured by monitoring the Soret band after addition of H_2O_2 (Fig. 9). As evident from the figure, a significant shielding of the heme molecule was seen by all forms of A1M, as compared to heme alone. This further supports a binding of the heme group to A1M. However, plotting the peak value of each A1M-form as a function of time (Fig. 9D) demonstrates a less efficient shielding of the heme-molecule in C34S-A1M as compared to Wt-A1M and the other two mutants. This suggests that the C34 residue is essential for the heme coordination and/or redox activities of the bound heme-groups.

3.6. Induced visible CD support binding of two heme-groups

Neither heme nor A1M alone exhibits any CD activity in the visible range (not shown). However, when a small aliquot of heme solution is added to A1M, a CD activity in the heme absorbance region (390–415 nm) was induced (so called Cotton Effect) for each A1M variant (Fig. 10). These results support binding of heme to all A1M-variants. Titrations of heme were also consistent with the presence of two binding sites, as reported previously [24]. At low heme concentrations (see bottom traces in Fig. 9, heme:A1M molar ratio 0.1), the induced CD proceeded to an equilibrium state relatively fast (<40 min), suggesting binding to the primary binding site. As summarized in Table 3, the peak wavelengths of the induced CD for Wt-A1M was 421 nm, and 417 nm, 397 nm and 416 nm for K [3]T-A1M, C34S-A1M and H123S-A1M, respectively, suggesting a different microenvironment of the heme molecule in the first binding site of each mutant. At higher heme concentrations (heme:A1M molar ratio 1.0; see upper traces in Fig. 10) the reaction was slower (>5 h to obtain equilibrium), consistent with binding at the second binding site at higher concentrations. The peak wavelengths (Table 3) of the induced CD at heme:A1M ratio 1.0 were different from those shown for heme:A1M ratio 0.1, suggesting different heme environments and/or coordination at the primary and secondary binding sites.

3.7. Molecular simulation of A1M-heme binding

The lipocalin pocket, as identified by CASTp, essentially encompasses the inner cavity of the protein with a molecular volume of 2033 Å^3. It was found that the inner lining of the pocket was composed of 41 residues. Apparently the molecular volume of heme, which is 538.9 Å^3, could readily fit inside the lipocalin pocket (Fig. 11).

Before proceeding with the docking of heme to A1M, it is pertinent to explore the binding modality of other members of the lipocalin family that are known to bind heme. A total of 45 nitrophorin 1, 2 or 4 structures from *Rhodnius prolixus* were obtained from the PDB. These members of the lipocalin family had amino acid length in the range of 179–184 and their superimposition performed using MultiProt indicated high structural homology affording an RMSD value of 1.91 Å (Fig. 12). Analysis of these structures revealed that the bound heme was coordinated to axial H59 and ammonia ligands in nearly all cases.

Heme was docked to A1M using default parameters of HADDOCK without explicit definition of active and passive residues as they were

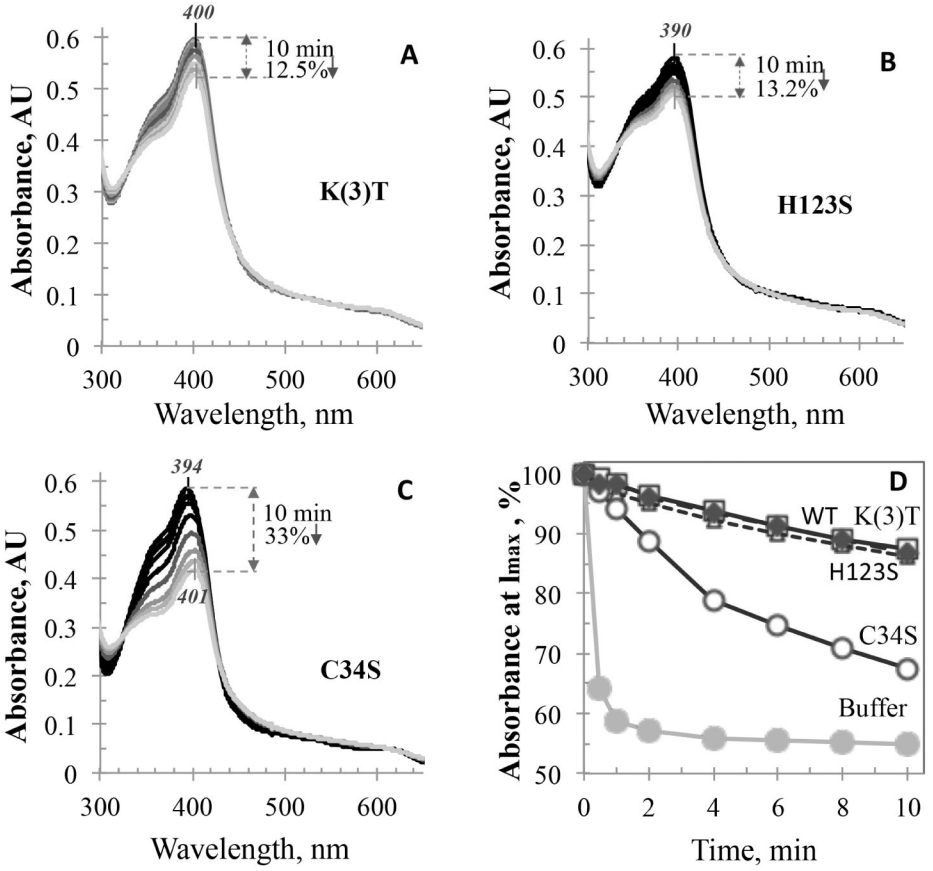

Fig. 9. Time-course UV/Vis absorbance data for catalase-like activity of the heme complexes with A1M mutants: (A) K [3]T; (B) H123S, and (C) C34S. The upper trace of each plot shows initial absorbance spectrum of each heme/mutant sample (1:1) as recorded over 10 min with time points taken at 30 s, 1 min, 2 min, 4 min, 6 min, 8 min, and 10 min after adding a 7 μl aliquot of 50 mM H_2O_2 stock solution to 1 ml of the protein sample. Plot (D) shows the percentage of the remaining intensity of the Soret band of each mutant in comparison with 0 s.

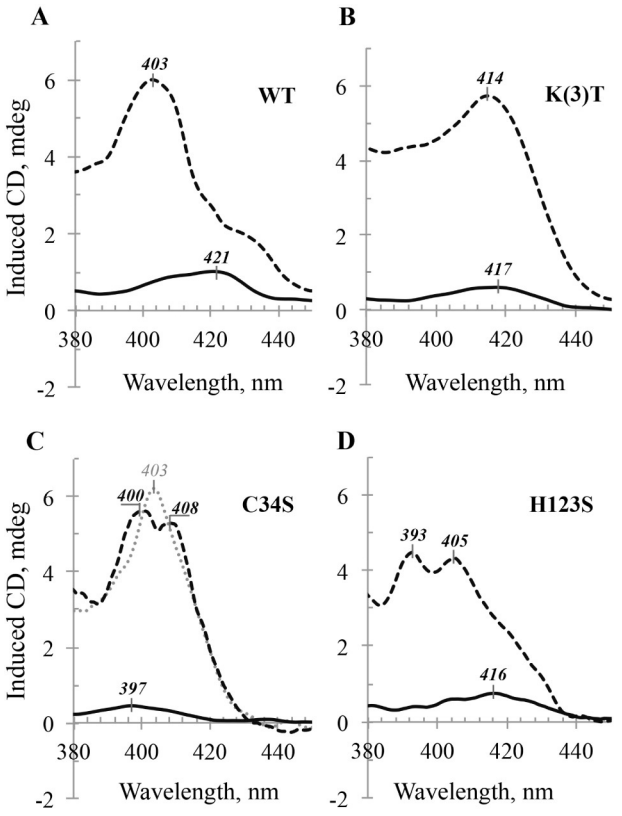

Fig. 10. Induced CD data for heme complexes with A1M. Wt-A1M (A), and A1M mutants K[3]T (B), C34S (C), and H123S (D). Induced CD spectra are shown for heme:A1M ratio 0.1 (solid traces in A-D, the spectra were recorded at 1 h after adding heme, when no additional spectral changes were observed) and heme:A1M ratio 1.0 (broken traces, measured 20 h after adding heme, when no additional changes were observed). The broken trace in 9A was previously published in Karnaukhova et al. [43]. Gray dotted trace shown for C34S plot (C) corresponds to an intermediate state observed for this C34S mutant at L/P 1.0 at the time point 1.5 h after adding heme. Protein concentration in all samples was 45 μM.

assigned automatically. Active residues correspond to residues that are directly involved in the interaction whereas the passive residues denote residues that are in the vicinity of active residues. A typical docking simulation is comprised of the following steps: (i) rigid-body docking, (ii) scoring and filtering, (iii) semi-flexible refinement, (iv) water refinement, (v) scoring and analysis and finally (vi) clustering of docked structures. Docking results indicated that there were 193 structures in 6 clusters and that the top-performing cluster was the most populated with 142 structures affording a HADDOCK score of -86.7 ± 7.9 and that the RMSD from the overall lowest-energy structure was 0.5 ± 0.3 indicative of the close similarity of the docking conformation among members of this cluster. Thus, the lowest-energy structure of the A1M-heme complex was selected for further comparison with a representative structure from the aforementioned set of 45 structures from *R. prolixus* (PDB ID: 1X8P) obtained at an ultrahigh resolution of 0.85 Å. Superimposition of the two structures yielded an RMSD of 12.37 Å spanning the entire length of 164 residues in A1M (Fig. 13).

It can be seen that the bound heme in A1M leaves the putative outer heme binding site available. To investigate whether this site could accommodate another heme, a subsequent docking procedure was performed using PyMOL such that the iron atom of the second heme was coordinated to the Sγ of C34 and Nε of H123. After structural refinement using energy minimization and MD simulation, the final model was compared with the crystal structure of wild-type A1M (PDB ID: 3QKG; resolution of 2.3 Å) [25]. A similar fold between the 3QKG structure and our heme-bound A1M model was observed with an RMSD of 1.29 Å (Fig. 14). The first heme binding site comprises residues from several strands of the β-barrel while the second heme binding site is formed by a few residues from the short α-helix at the open end and H123, which lies on loop 4, just opposite to the helix. Analyses of Ramachandran plot revealed that only 1.4% of A1M residues were located in the disallowed region (data not shown) thereby indicating that appropriate stereochemical quality of the heme-bound A1M model was achieved.

To investigate fluctuations of the A1M structure upon heme binding and interactions of hemes with their pockets, MD simulations were performed for 30 ns on both heme-bound and heme-free A1M structures using explicit-solvent periodic boundary conditions. Stability of the protein and heme structures over the course of the simulation was observed by measuring the time evolution of root mean square deviation (RMSD) with respect to their initial structures (Fig. 15A). It can be seen that the simulated structures of A1M reached equilibrium prior to $t = 5$ ns and remained stable throughout the simulation for both heme-bound and heme-free A1M models. RMSDs of the heme-bound A1M structure fluctuated around 0.2 nm whereas the heme-free A1M was slightly larger by ≈0.1 nm, which implies that heme molecules were pertinent in stabilizing the A1M structure. The RMSD as a function of time for hemes in the A1M-heme simulation was also investigated. It was found that the second heme fluctuated to a much greater extent than the first heme in which RMSDs were 0.412 ± 0.010 nm for the former and 0.141 ± 0.003 nm for the latter (Fig.15B). Such differences may suggest either large flexibility of the binding pocket for the second heme or a reflection of the different binding strengths afforded by the two hemes.

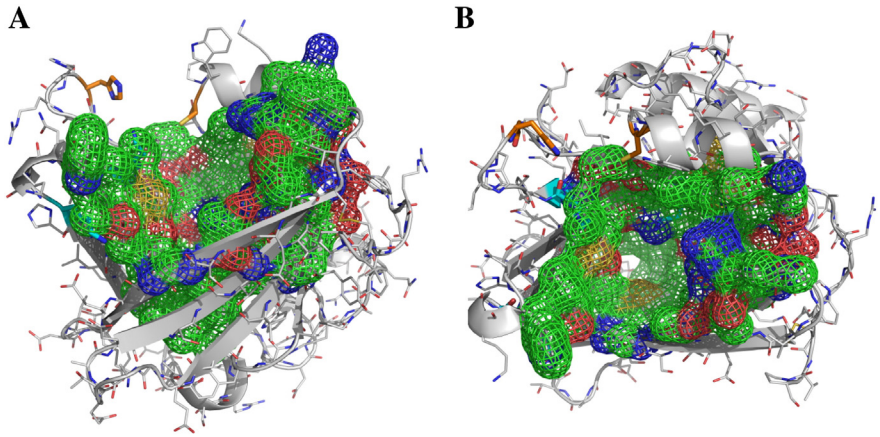

Fig. 11. Identified pocket in the crystal structure of A1M. Residues lining the pocket are represented as meshes and color coded by their constituent carbon, nitrogen and oxygen atoms as green, blue and red, respectively. Residues C34 and H123 are shown in orange whereas residues K92, K118 and K130 in cyan. Secondary structure and remaining side chain carbon atoms are displayed in white. Structures are shown from the side (A) and top (B) views.

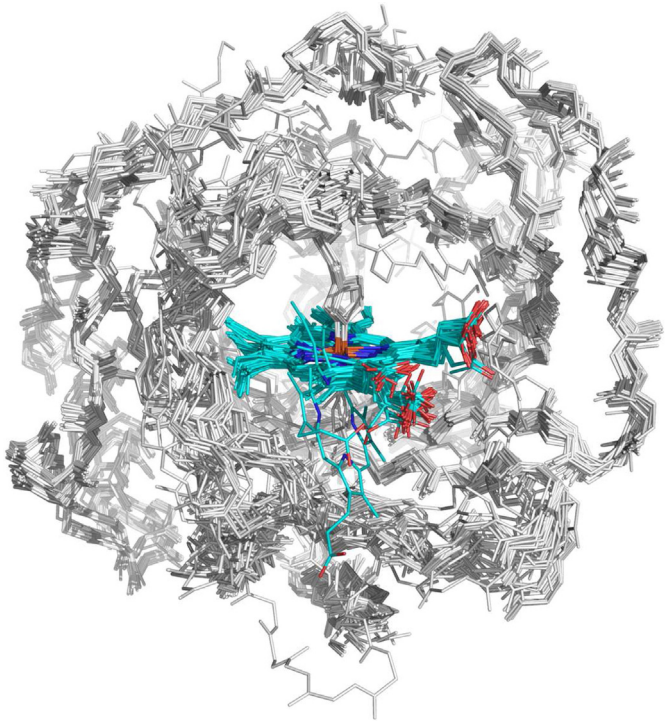

Fig. 12. Structural superimposition of 45 heme-nitrophorin complexes from *R. proxilus*. Carbon backbone are color coded as cyan color for heme moiety and white color for the protein structure. Nitrogen and oxygen atoms are color coded as blue and red, respectively, while the iron atom of the heme moiety is shown in orange color.

To assess the conformational flexibility of A1M with respect to individual structural regions of the protein, root mean square fluctuation (RMSF) of the backbone as a function of the residue number was measured in both simulations from $t = 5$ to 30 ns (Fig. 15C). It can be seen that in the free A1M simulation, the four loops connecting neighboring β-strands (designated loop-1 to −4) at the open end of the eight-stranded β-barrel exhibited considerably high flexibility. This result is consistent with the experimental data in that those regions displayed high crystallographic B-factors, except for loop-4 of the 3QKG structure, which is responsible for the metal-binding site as well as exhibiting low temperature factor [25]. As expected, presence of the second heme significantly decreased fluctuation of the binding site formed by the short α-helix of loop-1 (C34 to M40) and residues on loop-4 (S120 to G124). On the other hand, binding of the first heme did not alter the fluctuation of the lipocalin pocket in which a similar RMSF profile was observed in such region.

To investigate contributing factors that dominate the interaction of the A1M-heme complex, potential energies for interactions between each heme molecule and the protein were calculated as the sum of the electrostatic and van der Waals (vdW) interactions from $t = 5$ to 30 ns (Fig. 15D). It can be seen that the first heme exhibited considerably large negative interaction energies with the protein, which is in contrast to the second heme that exhibited lower interactions. It should be noted that electrostatic energies were found to be major factors stabilizing the interaction between the first heme and A1M while vdW interactions contributed more dominantly in the second heme-bound A1M. These results suggest that the first heme binds the lipocalin pocket of A1M with more strength than the second heme, which may explain the higher degree of flexibility of the heme molecule when bound to the second binding pocket of A1M. The aforementioned evidences also suggest that binding of the first heme to the lipocalin pocket stabilizes the protein structure and predisposes A1M for binding of the second heme to the surface-exposed binding site.

4. Discussion

4.1. Side-groups of C34, H123, K92, K118 and K130 are involved in heme-binding

The investigation in this paper is based on site-directed mutagenesis, *i.e.* biochemical analysis of wild-type A1M and three mutated forms of the protein. In order to ascertain that functional differences were due to the amino acid substitutions rather than impurities or effects of incorrect folding, we first investigated biochemical properties of the recombinant A1M-species. The proteins appeared highly purified, and far-UV CD spectra of Wt-A1M and the mutated A1M-forms suggested a similar composition of secondary structure, *i.e.* mostly β-structure (Fig. 2B; Table 1), consistent with the X-ray crystallography-derived three-dimensional structure of Wt-A1M [25]. Tryptophan fluorescence spectra were also recorded as an estimate of the overall conformation of the mutants (Fig. 2C). The C [34]S-mutant displayed a higher fluorescence intensity than Wt-A1M and the other mutants. Sulfur-containing molecules are known fluorescence quenchers [45]. The C34-residue and one of the four tryptophan residues, W36, are located closely together on the small helix on the rim of the lipocalin pocket (Fig. 1), hence there is a possibility of an interaction between these two residues reducing the intensity of the fluorescence of W36 in Wt-A1M and the other mutants. Apart from this, similar spectra were obtained, suggesting no major differences in the overall conformation of the four variants.

It was previously shown that heme binds specifically to A1M and that this feature is evolutionally conserved [21–23]. Furthermore, it was shown that A1M forms a trimeric complex with heme in a 1:2 stoichiometry [24]. In order to understand the mechanism of heme binding of A1M, the binding was studied by several different techniques, and to understand the structural requirements of the binding and possibly localize binding sites, the binding to mutated variants was also studied. In short, all methods showed that heme was bound to all variants and

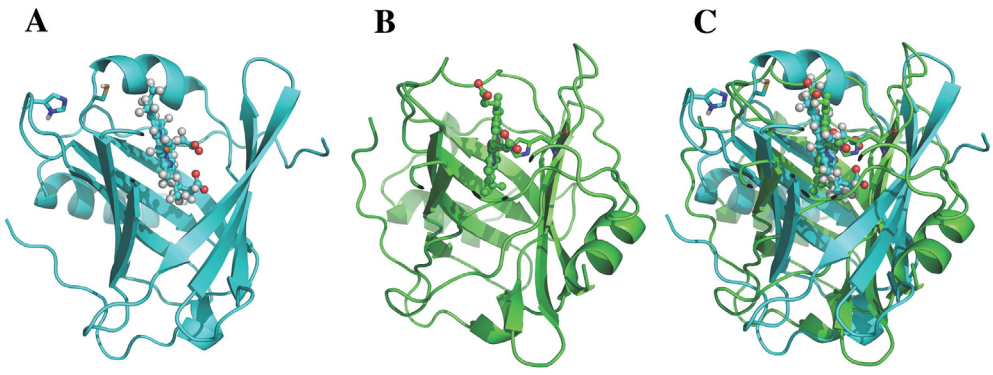

Fig. 13. Structures of heme complexes with A1M (A), nitrophorin 4 from *R. prolixus* (B) and superimposition of both A1M and nitrophorin 4-heme complexes (C). Carbon atoms are shown in cyan and green colors in panel A and B, respectively, while oxygen and hydrogen atoms are shown in red and white, respectively.

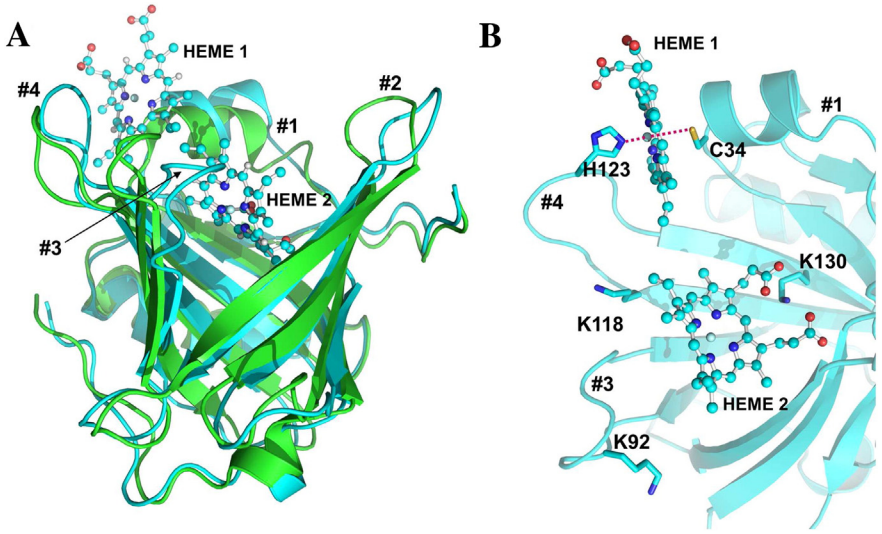

Fig. 14. Modeling of binding of two heme-molecules to A1M. Superimposition between the structure of A1M complexed with 2 heme molecules and the 3QKG structure of apo-A1M (A), and a close view of two different heme binding sites of A1M (B), heme molecules are represented in a ball and stick model, coordinated residues are shown as sticks and magenta lines indicate the coordination. The four loops are labeled #1–#4.

indicated a slightly higher binding by Wt-A1M compared to the mutated variants, whereas heme titration during CD-spectral analysis, UV–Vis absorbance spectrophotometry and the catalase-like activity assays revealed differences between the four A1M-variants suggesting involvement of the C34-, H123- and K(92,118,130)-side-groups.

The experimental results in this investigation were obtained using A1M of all four variants carrying an N-terminal His_8-tag. We used the migration shift-PAGE assay to show that non-tagged Wt-A1M binds the heme-group with similar binding strength [43]. Moreover, the results from SPR-analysis were obtained by studying A1M-molecules immobilized to the surface by binding *via* the His-tag. It was also shown previously that the His-tag does not contribute to, or interfere with, the reductase activities of A1M [19,20] and we therefore expect that any reductase activity of the A1M-variants in this investigation is not affected by the His-tag. Although this does not rule out that the His-tag may influence the heme binding, we therefore believe that the major conclusions of the work also are valid for non-tagged A1M.

4.2. Characterization of two heme-binding sites in A1M

Several different results suggest that each A1M molecule can bind two heme-groups simultaneously. A previous report used heme-titration, gel chromatography, and resonance Raman and EPR spectroscopy to demonstrate the formation of A1M:heme complexes with the stoichiometry 1:2 [24]. In the present work, the differences in the heme-induced CD-spectra at low and high heme:A1M ratios are consistent with a subsequent filling of two binding-sites. Based on the spectral behavior of the four A1M-variants, we propose that one heme binding site is located in the lipocalin pocket, the other is located between loops 1 and 4 at the outer rim of the pocket, and that the sites are filled in that order by increasing heme concentrations. The existence of an inner binding site is supported experimentally by the almost complete quenching of the tryptophan fluorescence in spite of the fact that one of the tryptophan residues (W25) is located at the bottom of the pocket, and the dependence of the heme-induced visual CD spectra on the K(92, 118, 130) residues which line the interior pocket wall. The outer binding site is supported by the influence of the C34- and H123-residues on heme-titration effects, the less efficient shielding of the heme-group from H_2O_2-induced degradation in the C34S-mutant, and was also proposed by Meining and Skerra [25] based on its similarities with a group of heme binding proteins with a Cys-Pro dipeptide motif [46].

Our *in silico* modeling supports the possibility of simultaneous binding of two heme-groups to the proposed inner and outer binding site. The inner binding site is analogous to the heme binding sites of nitrophorins, heme binding members of the Lipocalin protein family. Dynamic analysis of the models also suggests a stronger binding of heme to the inner binding site, and/or a higher flexibility of the second binding site. This is consistent with a primary binding to the inner site and a secondary binding to the outer binding site. Interestingly, the inner binding site suggests close proximity between K118 and K130 side-groups and the non-pyrrolic groups of the heme-molecule (Fig. 14B), supporting the differences in heme-induced visual CD-spectra between Wt- and K(92,118,130)T-A1M. It has previously been shown that these three side-groups become covalently modified and cross-linked *in vivo* by yellow-brown, unidentified, size heterogeneous compounds with molecular masses between 122 and 282 amu [47]. Based on this, it can be speculated that a reaction between the inner heme group and the A1M protein leads to degradation of the heme-group, yielding covalent attachment of degradation products to the lysyl side-chains. This hypothetical reaction may involve electron-transfer reactions of the iron atoms of both heme-groups as well as the thiol group of C34.

4.3. Possible electron transfer reaction between A1M and heme

The UV–Vis absorbance spectrum of Wt-A1M displayed the characteristic features of hemoglobin in its reduced form, *i.e.* a red-shifted Soret band and a peak at 540 nm, in contrast to the three mutated A1M forms (Fig. 9). A negative reduction potential of the C34 thiol group in combination with the three lysyl residues K92,118 and 130 was previously shown, *i.e.* A1M reduced methemoglobin, cytochrome c and free iron [19]. It may therefore be speculated that Wt-A1M keeps the outer heme-group in its reduced, ferrous (Fe2+) form by a tentative reaction that involves coordination of the iron atom by the C34- and H123-residues, where the C34 thiol group also may serve as an electron-source. As proposed earlier, the K(92,118,130)-residues may regulate the electronegativity of the thiol group by creating a positive electrostatic microenvironment [7,19].

4.4. Physiological function of heme-binding to A1M

Several potential physiological functions of the heme binding by A1M are possible. The first, and perhaps most obvious, may be

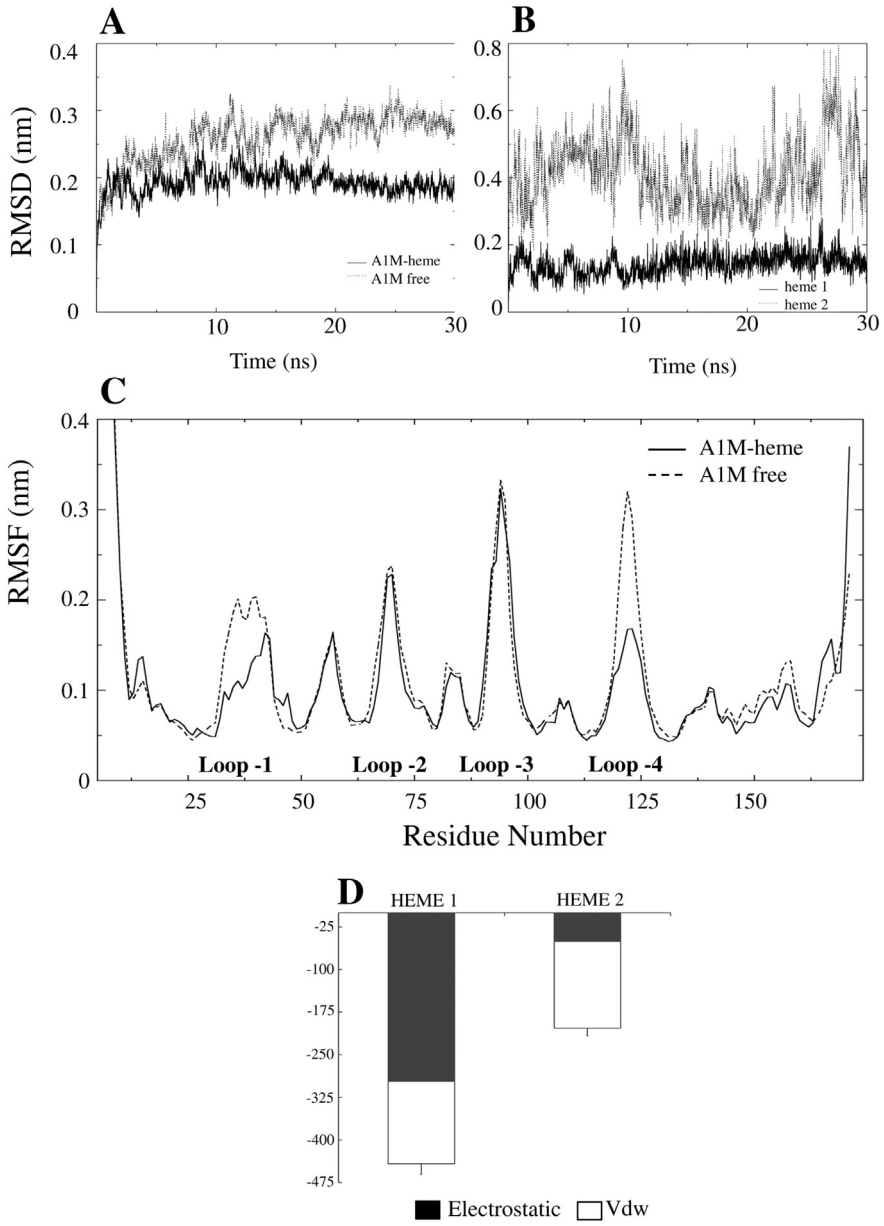

Fig. 15. MD simulation data of A1M-heme complexes. (A) Time evolution of root mean square deviation (RMSD) with respect to the initial structure for the protein backbone atoms and (B) the heavy atoms of heme molecules. (C) Backbone root mean square fluctuation (RMSF) for each amino acid residue from MD simulations of heme-bound and heme-free structures of A1M. (D) Potential energies for interactions between A1M and each heme molecule. The electrostatic and vdW contributions are shown in black and white, respectively. Error bars represent the standard deviation in the sum of the interactions.

scavenging of free heme-groups to protect biomolecules from heme-induced toxic reactions. This function is supported by previous reports that A1M-binding of heme results in inhibition of cell-lysis, cell-cycle arrest and molecular damage otherwise induced by the free heme [13,48]. Second, heme binding can be the first step in a series of reactions leading to *heme-degradation*. This also involves proteolytic cleavage of the C-terminal tetrapeptide Leu-Ile-Pro-Arg (pos 179–183) of A1M, as suggested in the report by Allhorn et al. [21]. However, nothing is known about the detailed molecular mechanisms leading to the heme-degradation. The position of the C-terminus beyond amino acid residue Gly172 could not be determined in the published crystal structure of A1M [25] and it is therefore difficult to speculate on the mechanistic influence of the C-terminal tetrapeptide on binding and degradation of the heme-group. Thirdly, the heme-group, with the iron atom, may be employed as an *enzymatic cofactor* during the redox activities of A1M. Heme-groups are commonly employed as electron-active cofactors in peroxidases, reductases, dehydrogenases, *etc.*, and it is therefore reasonable to imagine a role of the bound heme-groups in A1M in reduction, radical scavenging, or other antioxidative activities. This remains to be tested experimentally, however.

The concentration of A1M in blood plasma is 1–2 μM. Among heme binders in plasma, A1M is apparently not the strongest. Hemopexin has a much higher affinity. Albumin, which binds heme with a slightly higher affinity than A1M is much more abundant in blood. This suggests that the role of A1M is not primarily as a heme-scavenger in blood. A1M is secreted to blood from the liver, but rapidly transferred to the extravascular space ($T1/2 = 2.5$ min). The protein is also synthesized by most other epithelial cells and found both intracellularly and in the extracellular matrix, for example in skin and placenta. We therefore propose that the heme-reaction mechanisms of A1M are different from those of hemopexin and albumin, and of physiological importance in cells and extravascular fluids rather than in blood.

5. Conclusions

Several previous investigations have shown that the lipocalin A1M can bind to heme groups, and that this property constitutes part of its physiological antioxidative mechanisms [13,21,23]. In this work we have investigated the structural requirements of the heme binding. The main conclusions of the present report are that two heme-groups can be accommodated simultaneously in the protein, and that the binding and reactions with the heme-groups are affected by the Cys34, Lys92, 118, 130, and His123 residues lining the lipocalin pocket.

Conflicts of interest

Bo Åkerström is a founder and share-holder of A1M Pharma AB which holds patent rights on medical uses of A1M based on its heme-binding properties.

Acknowledgments

SR, LWR and BÅ are indebted to Maria E Johansson for invaluable technical assistance. This work was supported by the Swedish Medical Research Council (VR), governmental ALF research grants to Lund University and Lund University Hospital, the Royal Physiographic Society in Lund, the Foundations of Greta and Johan Kock, Alfred Österlund, the Blood and Defense Network, Lund University, the Crafoord Foundation (20081029) and A1M Pharma AB. CN is supported by a Research Career Development Grant (No. RSA5780031) from the Thailand Research Fund. AIA acknowledges the support from the National Institutes of Health (NIH) under grants HL110900 and the U.S. Food and Drug Administration (MODSCI Grants).

References

[1] D.R. Flower, The lipocalin protein family: structure and function, Biochem. J. 318 (Pt 1) (1996) 1–14.
[2] B. Åkerström, D.R. Flower, J.P. Salier, Lipocalins: unity in diversity, Biochim. Biophys. Acta 1482 (2000) 1–8.
[3] B. Åkerström, N. Borregaard, D.R. Flower, J.P. Salier (Eds.), *Lipocalins*: *An Introduction*, Landers Bioscience, Georgetown, Texas, 2006.
[4] M.D. Ganfornina, D. Sanchez, L.H. Greene, D.R. Flower (Eds.), *The Lipocalin Protein Family*: *Protein Sequence*, *Structure and Relationship to the Calycin Superfamily*, Landers Bioscience, Georgetown, Texas, 2006.
[5] B. Ekström, I. Berggård, Human α1-microglobulin. Purification procedure, chemical and physiochemical properties, J. Biol. Chem. 252 (1977) 8048–8057.
[6] B. Åkerström, L. Lögdberg, An intriguing member of the lipocalin protein family: a_1-microglobulin, Trends Biochem. Sci. 15 (1990) 240–243.
[7] B. Åkerström, M. Gram, A1M, an extravascular tissue cleaning and housekeeping protein, Free Radic. Biol. Med. 74 (2014) 274–282.
[8] J.F. Kaumeyer, J.O. Polazzi, M.P. Kotick, The mRNA for a proteinase inhibitor related to the HI-30 domain of inter-alpha-trypsin inhibitor also encodes a_1-microglobulin (protein HC), Nucleic Acids Res. 14 (1986) 7839–7850.
[9] A. Lindqvist, T. Bratt, M. Altieri, W. Kastern, B. Åkerström, Rat alpha 1-microglobulin: co-expression in liver with the light chain of inter-alpha-trypsin inhibitor, Biochim. Biophys. Acta 1130 (1992) 63–67.
[10] T. Bratt, H. Olsson, E.M. Sjöberg, B. Jergil, B. Åkerström, Cleavage of the alpha 1-microglobulin-bikunin precursor is localized to the Golgi apparatus of rat liver cells, Biochim. Biophys. Acta 1157 (1993) 147–154.
[11] A. Grubb, E. Mendez, J.L. Fernandez-Luna, C. Lopez, E. Mihaesco, J.P. Vaerman, The molecular organization of the protein HC-IgA complex (HC-IgA), J. Biol. Chem. 261 (1986) 14313–14320.
[12] T. Berggård, N. Thelin, C. Falkenberg, J.J. Enghild, B. Åkerström, Prothrombin, albumin and immunoglobulin A form covalent complexes with alpha1-microglobulin in human plasma, Eur. J. Biochem. 245 (1997) 676–683.
[13] M.G. Olsson, T. Olofsson, H. Tapper, B. Åkerström, The lipocalin alpha1-microglobulin protects erythroid K562 cells against oxidative damage induced by heme and reactive oxygen species, Free Radic. Res. 42 (2008) 725–736.
[14] M.G. Olsson, M. Allhorn, J. Larsson, M. Cederlund, K. Lundqvist, A. Schmidtchen, O.E. Sörensen, M. Mörgelin, B. Åkerström, Up-regulation of A1M/a_1-microglobulin in skin by heme and reactive oxygen species gives protection from oxidative damage, PLoS One 6 (2011), e27505.
[15] K. May, L. Rosenlöf, M.G. Olsson, M. Centlow, M. Mörgelin, I. Larsson, M. Cederlund, S. Rutardottir, W. Siegmund, H. Schneider, B. Åkerström, S.R. Hansson, Perfusion of human placenta with hemoglobin introduces preeclampsia-like injuries that are prevented by alpha1-microglobulin, Placenta 32 (2011) 323–332.
[16] L. Wester-Rosenlöf, V. Casslen, J. Axelsson, A. Edström-Hägerwall, M. Gram, M. Holmqvist, M.E. Johansson, I. Larsson, D. Ley, K. Marsal, M. Mörgelin, B. Rippe, S. Rutardottir, B. Shohani, B. Åkerström, S.R. Hansson, A1M/alpha1-microglobulin protects from heme-induced placental and renal damage in a pregnant sheep model of preeclampsia, PLoS One 9 (2014), e86353.
[17] K. Sverrisson, J. Axelsson, A. Rippe, M. Gram, B. Åkerström, S.R. Hansson, B. Rippe, Extracellular fetal hemoglobin induces increases in glomerular permeability: inhibition with alpha1-microglobulin and tempol, Am. J. Physiol. Ren. Physiol. 306 (2014) F442–F448.
[18] S. Rutardottir, E.J. Nilsson, J. Pallon, M. Gram, B. Åkerström, The cysteine 34 residue of A1M/alpha1-microglobulin is essential for protection of irradiated cell cultures and reduction of carbonyl groups, Free Radic. Res. 47 (2013) 541–550.
[19] M. Allhorn, A. Klapyta, B. Åkerström, Redox properties of the lipocalin alpha1-microglobulin: reduction of cytochrome c, hemoglobin, and free iron, Free Radic. Biol. Med. 38 (2005) 557–567.
[20] B. Åkerström, G.J. Maghzal, C.C. Winterbourn, A.J. Kettle, The lipocalin alpha1-microglobulin has radical scavenging activity, J. Biol. Chem. 282 (2007) 31493–31503.
[21] M. Allhorn, T. Berggård, J. Nordberg, M.L. Olsson, B. Åkerström, Processing of the lipocalin α1-microglobulin by hemoglobin induces heme-binding and heme-degradation properties, Blood 99 (2002) 1894–1901.
[22] M. Allhorn, K. Lundqvist, A. Schmidtchen, B. Åkerström, Heme-scavenging role of α1-microglobulin in chronic ulcers, J. Investig. Dermatol. 121 (2003) 640–646.
[23] J. Larsson, M. Allhorn, B. Åkerström, The lipocalin α1-microglobulin binds heme in different species, Arch. Biochem. Biophys. 432 (2004) 196–204.
[24] J.F. Siebel, R.L. Kosinsky, B. Åkerström, M. Knipp, Insertion of heme b into the structure of the Cys34-carbamidomethylated human lipocalin alpha(1)-microglobulin: formation of a [(heme)(2) (alpha(1)-microglobulin)](3) complex, Chembiochem 13 (2012) 879–887.
[25] W. Meining, A. Skerra, The crystal structure of human alpha(1)-microglobulin reveals a potential haem-binding site, Biochem. J. 445 (2012) 175–182.
[26] T. Finkel, N.J. Holbrook, Oxidants, oxidative stress and the biology of ageing, Nature 408 (2000) 239–247.
[27] A. Kwasek, P. Osmark, M. Allhorn, A. Lindqvist, B. Åkerström, Z. Wasylewski, Production of recombinant human alpha1-microglobulin and mutant forms involved in chromophore formation, Protein Expr. Purif. 53 (2007) 145–152.
[28] Lamar.colostate.edu/~/sreeram/CDPro/.
[29] E. Karnaukhova, S.S. Krupnikova, M. Rajabi, A.I. Alayash, Heme binding to human alpha-1 proteinase inhibitor, Biochim. Biophys. Acta 1820 (2012) 2020–2029.
[30] EMBL, European Bioninformatics Institute, P, 2014.
[31] Molinspiration, C. o. M. P. a. B. S. (2014).
[32] Molinspiration, M. v. (2014).
[33] W, D, PyMOL Release 0.99, DeLano Scientific LLC, Palo Alto, 2002.
[34] J. Dundas, Z. Ouyang, J. Tseng, A. Binkowski, Y. Turpaz, J. Liang, CASTp: computed atlas of surface topography of proteins with structural and topographical mapping of functionally annotated residues, Nucleic Acids Res. 34 (2006) W116–W118.
[35] M. Shatsky, R. Nussinov, H.J. Wolfson, A method for simultaneous alignment of multiple protein structures, Proteins 56 (2004) 143–156.
[36] S.J. de Vries, M. van Dijk, A.M. Bonvin, The HADDOCK web server for data-driven biomolecular docking, Nat. Protoc. 5 (2010) 883–897.
[37] D. Van Der Spoel, E. Lindahl, B. Hess, G. Groenhof, A.E. Mark, H.J. Berendsen, GROMACS: fast, flexible, and free, J. Comput. Chem. 26 (2005) 1701–1718.
[38] H.J.C. Berendsen, J.P.M. Postma, W.F. Van Gunsteren, A. Dinola, J.R. Haak, Molecular dynamics with coupling to an external bath, J. Chem. Phys 81 (1984) 3684.
[39] M. Parinello, A. Rahman, Polymorphic transitions in single crystals: a new molecular dynamics method, J. Appl. Phys. 52 (1981) 7182.
[40] C. Oostenbrink, A. Villa, A.E. Mark, W.F. van Gunsteren, A biomolecular force field based on the free enthalpy of hydration and solvation: the GROMOS force-field parameter sets 53A5 and 53A6, J. Comput. Chem. 25 (2004) 1656–1676.
[41] B. Hess, H. Bekker, H.J. Berendsen, J.G.E.M. Fraaije, LINCS: a linear constraint solver for molecular simulations, J. Comput. Chem. 18 (1997) 1463–1472.
[42] T. Darden, D. York, L. Pedersen, Particle mesh Ewald: an N log(N) method for Ewald sums in large systems, J. Chem. Phys. 98 (1993).
[43] E. Karnaukhova, S. Rutardottir, M. Rajabi, L. Wester Rosenlöf, A.I. Alayash, B. Åkerström, Characterization of heme binding to recombinant alpha1-microglobulin, Front. Physiol. 5 (2014) 465.
[44] C.C. Winterbourn, Oxidative reactions of hemoglobin, Methods Enzymol. 186 (1990) 265–272.
[45] I.M. Kuznetsova, T.A. Yakusheva, K.K. Turoverov, Contribution of separate tryptophan residues to intrinsic fluorescence of actin. Analysis of 3D structure, FEBS Lett. 452 (1999) 205–210.
[46] T. Li, H.L. Bonkovsky, J.T. Guo, Structural analysis of heme proteins: implications for design and prediction, BMC Struct. Biol. 11 (2011) 13.
[47] T. Berggård, A. Cohen, P. Persson, A. Lindqvist, T. Cedervall, M. Silow, I.B. Thogersen, J.A. Jönsson, J.J. Enghild, B. Åkerström, a_1-microglobulin chromophores are located to three lysine residues semiburied in the lipocalin pocket and associated with a novel lipophilic compound, Protein Sci. 8 (1999) 2611–2620.
[48] M.G. Olsson, M. Allhorn, L. Bülow, S.R. Hansson, D. Ley, M.L. Olsson, A. Schmidtchen, B. Åkerström, Pathological conditions involving extracellular hemoglobin: molecular mechanisms, clinical significance, and novel therapeutic opportunities for alpha(1)-microglobulin, Antioxid. Redox Signal. 17 (2012) 813–846.